

Photo-induced semimetallic states realised in electron-hole coupled insulators

Kozo Okazaki^{1,*}, Yu Ogawa¹, Takeshi Suzuki¹, Takashi Yamamoto¹, Takashi Someya¹, Shoya Michimae¹, Mari Watanabe¹, Yangfan Lu², Minoru Nohara³, Hidenori Takagi^{2,4}, Naoyuki Katayama⁵, Hiroshi Sawa⁵, Masami Fujisawa¹, Teruto Kanai¹, Nobuhisa Ishii¹, Jiro Itatani¹, Takashi Mizokawa⁶, and Shik Shin^{1,*}

¹*Institute for Solid State Physics, University of Tokyo, Kashiwa, Chiba 277-8581, Japan*

²*Department of Physics, University of Tokyo, Bunkyo-ku, Tokyo 113-0033, Japan*

³*Research Institute for Interdisciplinary Science, Okayama University, Okayama 700-8530, Japan*

⁴*Max Planck Institute for Solid State Research, Heisenbergstrasse 1, 70569 Stuttgart, Germany*

⁵*Department of Applied Physics, Nagoya University, Nagoya 464-8603, Japan*

⁶*School of Advanced Science and Engineering, Waseda University, Shinjuku-ku, Tokyo 169-8555, Japan*

*To whom correspondence should be addressed. E-mail: okazaki@issp.u-tokyo.ac.jp; shin@issp.u-tokyo.ac.jp.

Using light to manipulate materials into desired states is one of the goals in condensed matter physics, since light control can provide ultrafast and environmentally-friendly photonics devices. However, it is generally difficult to realise a photo-induced phase which is not merely a higher entropy phase

corresponding to a high-temperature phase at equilibrium. Here, we report realization of photo-induced insulator-to-metal transitions in $\text{Ta}_2\text{Ni}(\text{Se}_{1-x}\text{S}_x)_5$ including the excitonic insulator phase using time- and angle-resolved photoemission spectroscopy. From the dynamic properties of the system, we determine that screening of excitonic correlations plays a key role in the timescale of the transition to the metallic phase, which supports the existence of an excitonic-insulator phase at equilibrium. The non-equilibrium metallic state observed unexpectedly in the direct-gap excitonic insulator opens up a new avenue to optical band engineering in electron-hole coupled systems.

Introduction.

In semimetals or small-gap semiconductors, valence-band holes and conduction-band electrons may form bound states or excitons via weakly screened Coulomb interaction. The excitons condensate in a Bardeen-Cooper-Schrieffer (BCS) or Bose-Einstein condensation (BEC) manner, depending on whether the electron-hole coupling is weak or strong, and such a ground state is theoretically predicted as an excitonic insulator¹. One of the prototypical candidates of excitonic insulators is $1T\text{-TiSe}_2$, which shows a charge-density-wave (CDW) transition accompanying a $2\times 2\times 2$ structural distortion at $\sim 202\text{ K}$ ^{2,3}. Figure 1a illustrates a canonical phase diagram of excitonic insulators, and $1T\text{-TiSe}_2$ indeed exhibits such a phase diagram. One of the most plausible evidence that $1T\text{-TiSe}_2$ is an excitonic insulator has been reported by Hellmann *et al*⁴. They have classified several CDW insulators by their dominant interactions to Mott, excitonic, and Peierls insulators based on their melting times of electronic order parameters by time- and angle-resolved photoemission spectroscopy. In addition, a recent electron energy loss spectroscopy study on $1T\text{-TiSe}_2$ has reported an electronic collective mode coupled to phonons expected for an excitonic insulator⁵. However, since $1T\text{-TiSe}_2$ has indirect-type electron and hole bands (the valence band maximum and the conduction band

minimum are located at different positions in the Brillouin zone), and its excitonic condensation is inevitably accompanied by a band folding with a finite wave vector q like a Peierls insulator, it is still difficult to exclude contribution of electron lattice interaction. Also the indirect gap is not favourable for optical control of electrons and holes for future application.

On the other hand, Ta_2NiSe_5 , which has been supposed to be a unique candidate of excitonic insulators in the strong coupling (BEC) regime, has a quasi-one-dimensional structure composed of layers of Ni single chains and Ta double chains along the a -axis (Fig. 1b), and each layer is stacked by van der Waals interactions^{6,7}. Hybridised Ni $3d$ and Se $4p$ orbitals mainly compose the valence band near the Fermi level (E_F), whereas Ta $5d$ orbitals primarily form the doubly degenerate conduction bands (Fig. 1c)^{6,7}. This degeneracy can be partially lifted by the finite hybridisation between the two Ta chains. When the temperature decreases, Ta_2NiSe_5 undergoes a semiconductor-to-insulator transition at 328 K, accompanied by a structural distortion from orthorhombic to monoclinic symmetry^{6,7,8}. According to the angle-resolved photoemission spectroscopy (ARPES) measurements in the equilibrium state, it has been found that the top portion of the valence band remarkably becomes flat below the transition temperature. This has been considered as evidence for the spontaneous formation of excitons between the Ta $5d$ electron bands and the Ni $3d$ -Se $4p$ hybridised hole bands and thus, a phase transition to an excitonic insulator in the strong coupling regime⁹⁻¹². Recently, Lu *et al.*, have established the phase diagram of $\text{Ta}_2\text{Ni}(\text{Se}_{1-x}\text{S}_x)_5$ which covers the excitonic insulator phase and the band insulator phase as a function of x ¹³. However, more direct evidence for the excitonic insulating phase is still lacking so far. If the similar behaviour of the pump-fluence dependence to the photo-excitation to $1T$ - TiSe_2 is observed also in Ta_2NiSe_5 , it will strengthen that the behaviour can be regarded as the evidence for the excitonic insulating phase.

For the present study, we have performed the measurements of time- and angle-resolved photoemission spectroscopy (ARPES) to obtain such evidence that Ta_2NiSe_5 is actually an excitonic insulator from its pump-fluence dependence of the photo-excitation dynamics. Whereas several time-resolved studies on Ta_2NiSe_5 have been reported so far¹⁴⁻¹⁷, the present study is quite unique in that we employ a pump laser with shorter pulse duration (~ 30 fs), and extreme ultra violet (XUV) laser from high harmonic generation for probe pulses. Whereas we have employed 1 kHz for the repetition rate of the laser in order to generate higher order harmonics, this makes higher pump fluence available compared to higher repetition rate with the same average power of pump pulses. This would be the reason why we obtained the rather different ARPES results from Mor *et al.*, which have revealed the band gap narrowing and the enhanced excitonic coupling in Ta_2NiSe_5 by photo-excitation¹⁵. We do observe that slightly S-substituted Ta_2NiSe_5 shows a characteristic pump-fluence dependence in its excitation dynamics, whereas Ta_2NiS_5 , which had been considered as an ordinary band insulator, shows no dependence. Furthermore, quite unexpectedly, we find a non-equilibrium metallic phase as a photo-excited state of slightly S-substituted Ta_2NiSe_5 as well as Ta_2NiS_5 . Whereas our results strongly suggest that Ta_2NiSe_5 is an excitonic insulator, our observation of non-equilibrium metallic phase in both of slightly S-substituted Ta_2NiSe_5 and Ta_2NiS_5 may require reconsidering that Ta_2NiS_5 is not an ordinary band insulator. We propose the importance of the electron correlation effect for the insulating ground state of Ta_2NiS_5 . In addition, our findings serve a new pathway to phase control of materials including excitonic insulators by light.

Results

Pump-fluence dependence

First, we demonstrate that Ta_2NiSe_5 (hereafter, 3% S-substituted Ta_2NiSe_5 used in this study is simply referred as Ta_2NiSe_5 , since the electronic structure is almost not

affected by the substitution as shown in Supplementary Fig. 2) shows a characteristic pump-fluence dependence to photo-excitation similar to another candidate of excitonic insulators, $1T\text{-TiSe}_2$. Figure 2a shows an energy-momentum (E - k) map around the Γ point (centre of the Brillouin zone) taken before the arrival of the pump pulse at 100 K. The overall features of the spectra are confirmed to be consistent with those of the spectrum taken at equilibrium, especially for the gap of ~ 250 meV, and this certifies that distortion of the spectra due to space charge effects, which could often occur for TARPES measurements with a low repetition frequency such as 1 kHz, has been minimized. After the arrival of the pump pulse, the spectral weight of the flat band immediately decreases and is transferred to the originally gapped region at E_F within 100 fs. This temporal evolution is shown in Fig. 2b. These dynamics are much faster than excess energy transfer from hot electrons to the cold phonon bath, which has been generally reported to require ~ 1 ps and are more likely to be associated with purely electronic process, which has been supposed to be ~ 100 fs or faster^{18, 19}. In order to visualize these dynamics of the flat band after photo-excitation, in Fig 2c we show the temporal evolution of the integrated TARPES intensity of the rectangular region in Fig. 2a as a function of the pump-probe delay (Δt) for several pump fluences. The initial decrease of the TARPES intensity strongly depends on the pump fluence and becomes faster with increasing pump fluence similar to the already reported $1T\text{-TiSe}_2$ (Refs. 4 and 20). In order to evaluate the drop time of the flat band (τ_{Flat}) (the time scale that the intensity of the flat band decreases after pumping) of Ta_2NiSe_5 , the data were fitted to a Gaussian-convoluted rise-and-decay function, similar to that used in Ref. 20, and the obtained values of τ_{Flat} are plotted as blue symbols in Fig. 2d.

The time scale of the gap collapse in excitonic insulators is considered to be inversely proportional to the plasma frequency, $\omega_p = (ne^2/\epsilon_0\epsilon_r m^*)^{1/2}$, where n is the carrier density, e is the elementary charge and m^* is the effective mass of the valence or conduction band, ϵ_0 is the electric constant, and ϵ_r is the dielectric constant^{4,20}. From this

relationship, the gap quenching time should be proportional to $1/\sqrt{n}$. Since the ground state of Ta_2NiSe_5 is an insulating phase and the carrier density n in the equilibrium state is expected to be quite small, the carrier density n in the photo-excited state is expected to be nearly proportional to the pump fluence. We found that the drop time τ_{flat} of Ta_2NiSe_5 was proportional to $1/F^{0.7}$, where F is the pump fluence (Fig. 2d). On the other hand, we have performed the similar measurements also on Ta_2NiS_5 and the results are shown in Supplementary Fig. 3. The drop time of the top portion of the valence band was deduced from the fitting, and is plotted as red symbols in Fig. 2d. Contrastingly, it does not show clear pump fluence dependence. Thus, our results strongly suggest that Ta_2NiSe_5 is an excitonic insulator, but Ta_2NiS_5 is not (The behaviour of Ta_2NiS_5 is discussed later again). At least, the band gap of Ta_2NiSe_5 appears to originate from an electronic mechanism similar to that of $1T\text{-TiSe}_2$.

Temporal evolution of TARPES spectra

Next, we show more impressive temporal evolution of TARPES spectra of Ta_2NiSe_5 . Figures 3a and 3b show the temporal evolution of the momentum-integrated energy distribution curve (EDC) and its integrated intensity above E_F , respectively. After the arrival of pump pulse, the intensity above E_F immediately increases and relaxes with a time constant of 620 fs, which was estimated from the fitting to a Gaussian-broadened exponential decay function. Figures 3c and 3d show TARPES snapshots acquired at several Δt values and their differential spectra which were obtained by subtracting the spectrum averaged for $\Delta t < 0$, respectively (see also Supplementary Movie 1). The most notable spectral change is the emergence of an electron-like band crossing E_F , which is clearly seen in red colour in Fig. 3d at $\Delta t = 150$ and 250 fs. In other words, the system changes from an insulating state into a metallic state by photoexcitation. Figure 3e shows the temporal evolution of the EDCs integrated in the momentum range $[-0.1, 0.1] \text{ \AA}^{-1}$. Before the pump pulse arrives, the flat band

appears as the strongest peak at $E-E_F \sim -250$ meV. Immediately after pumping ($\Delta t = 150$ fs), the flat band collapses and the spectral weight shifts towards higher energies. At $\Delta t = 250$ fs, the peak intensity of the flat band decreases remarkably compared to the peak at $E-E_F \sim -640$ meV. Meanwhile, the edge at E_F was found to follow the Fermi-Dirac distribution, and the electronic temperature was estimated from the fitting to be as high as ~ 720 K. Since the resistivity of Ta_2NiSe_5 has been reported to become metallic-like above ~ 550 K⁷, the observed metallic bands may correspond to this metallic behaviour at high temperature. However, this high-temperature metallic resistivity originates from thermally excited carriers and the band gap is expected to be finite even at high temperature¹³. Thus, the observed transient metallic phase could be entirely different from that observed at higher temperatures at equilibrium.

To examine the photo-induced metallic phase in more detail, we compare the time-integrated spectra before and after pumping shown in Figs. 4a and 4b, respectively. After photo-excitation, both the electron and hole bands cross E_F at the same Fermi momentum $k_F \sim 0.1 \text{ \AA}^{-1}$ as schematically shown by the red and blue parabolas in Fig. 4b [see Supplementary Figs. 4 and 5 for the analysis of EDCs and momentum distribution curves (MDCs) before and after pumping]. This may indicate that the hybridisation between the two Ta chains is sufficiently strong to lift the degeneracy. However, since this is not predicted by band-structure calculations¹⁰, this behaviour of the emerging of the hole and electron bands crossing E_F at the same k_F is a surprising nature of the observed non-equilibrium metallic phase, indicating that the observed non-equilibrium metallic state is entirely different from the high temperature phase in the equilibrium state.

To confirm that the observed non-equilibrium metallic phase of Ta_2NiSe_5 can be associated with the excitonic condensation, we have performed comparative TARPES measurements on Ta_2NiS_5 and the results are shown in Supplementary Fig. 6. Quite

unexpectedly, an electron band emerges above E_F and the hole band below E_F shifts upward. In addition, the bottom of the electron band and the top of the hole band seems to cross E_F , and the system seems likely to be semimetallic. This may require reconsidering the nature of the insulating phase for Ta_2NiS_5 , which had been considered as an ordinary band insulator¹², since the valence state of nickel and tantalum is naively considered as $\text{Ni}^{0+}(3d^{10})$ and $\text{Ta}^{5+}(5d^0)$. According to the band-structure calculation based on the density functional theory²¹, Ta_2NiS_5 as well as Ta_2NiSe_5 is predicted to be metallic. Hence, the electron correlation effect may be important for the origin of the band gap of Ta_2NiS_5 . Wakisaka *et al.*, has suggested this possibility for Ta_2NiSe_5 , and reported that the ground state of Ta_2NiSe_5 should have a significant contribution from a $d^9\bar{L}$ configuration of Ni^{2+} [the valence state of tantalum is $\text{Ta}^{4+}(5d^1)$], where \bar{L} denotes a hole in the Se $4p$ orbital⁹. Further, $\text{NiS}_{2-x}\text{Se}_x$ is known as a bandwidth-control metal-insulator transition system, where the band width is broadened by substitution of Se for S^{22, 23}. Similarly, the band width of the Ta_2NiS_5 is narrower than that of Ta_2NiSe_5 , and the electron correlation effect could be more important for the origin of the band gap of Ta_2NiS_5 . Taking account of this possibility, the drop time of the top portion of the valence band of Ta_2NiS_5 can be understood. For the Mott gap, of which origin is predominantly electron correlation effect, the time scale of the gap collapse is considered to be inversely proportional to the band width, and expected to be very fast⁴. Actually, the drop time of Ta_2NiS_5 seems to be faster than the temporal resolution of our TARPES measurements.

However, if the electronic configuration of nickel in Ta_2NiS_5 is close to $d^9\bar{L}$, this corresponds to that of tantalum close to $5d^1$, and mechanism for the insulating behaviour of Ta $5d$ electrons must be considered. One possibility is formation of singlet bonds between the localized Ni $3d$ spins and Ta $5d$ electrons as well as S $3p$ holes (a schematic energy diagram is shown in Supplementary Fig. 7). If one considers that Ta $5d$ electrons in the double chains form singlet states with the localized $d^9\bar{L}$ state via hybridization

with the S $3p$ orbitals, the ground state of Ta_2NiS_5 can be viewed as a valence-bond-like insulating state which is analogous to a Kondo insulating state. As suggested from the time scale of the gap collapse, the Mottness of the Ni $3d$ electrons increases from Se to S, and consequently, the nature of ground state is changed from the excitonic insulator to the valence-bond insulator²⁴.

Discussion

Lastly, we discuss the mechanism of the photo-induced insulator-to-metal transitions realised in Ta_2NiSe_5 and Ta_2NiS_5 . Whereas the dynamics of the gap collapse is governed by the interactions of the gap origin, the realization of the non-equilibrium metallic phase cannot be understood straightforward, because no high-temperature metallic phase exists at least for Ta_2NiS_5 . Recently, coherent phonon excitations coupled to the electronic Higgs mode has been found by the pump-probe optical measurements with the similar pump fluence to our TARPES measurements for Ta_2NiSe_5 ¹⁴. Also, an interesting relation between the observed coherent phonon excitations and temperature-dependent Raman spectra has been reported by Mor *et al.*¹⁶ The coherent phonon excitations observed in various systems²⁵⁻²⁷ are most likely explained by the displacive excitation of coherent phonons (DECP) mechanism²⁸. In this mechanism, the adiabatic energy potential is modified due to photo-excitations and has the minimum with the finite atomic displacements corresponding to the A_g phonon. The electronic structure could be modulated by these lattice displacements. The observed metallic phase could be a result from this modulation of the electronic structure. If the coherent phonons of the 3.7 and/or 4 THz mode found by Mor *et al.* were related to the observed photo-induced phase transitions, these modes give a time scale of ~ 130 fs from the half-cycle time of the oscillation. This time scale could be faster for Ta_2NiS_5 , because these modes are expected to include oscillations of Se atoms²⁹ and S is a lighter element than Se, and thus, regarded to be comparable to the

observed gap collapse. If the observed metallic phase is driven by the modulation of the electronic structure due to the coherent lattice displacements, whereas incoherent lattice displacements driven by a large electronic density redistribution due to the strong pump pulses also could induce such modulation, as schematically shown in Fig. 1a, the observed photo-induced transition cannot correspond to the dashed vertical arrow, but may rather correspond to the solid arrow. At least, as described above, the non-equilibrium metallic phases observed for both of Ta_2NiSe_5 and Ta_2NiS_5 should suggest that these photo-induced phase transitions are not merely transitions to higher entropy states that can be realised at high temperatures in the equilibrium state, but correspond to the dashed vertical arrow in Fig. 1a. Thus, photo-excitation can induce similar effects to pressure, and as the pressure-induced superconducting phase has been found for Ta_2NiSe_5 , with some appropriate pumping condition probably with lower photon energy of some resonant condition, which would not give too much electronic entropy to the system, photo-induced superconductivity might be realised for this material. Realisation of this fascinating photo-induced phase would be one of the ultimate goals of investigations of the photo-excited electronic state.

Methods

Sample preparation. High-quality single crystals of $\text{Ta}_2\text{Ni}(\text{Se}_{0.97}\text{S}_{0.03})_5$ and Ta_2NiS_5 were grown by the chemical vapour transport method. Whereas the relatively large cleaved surface is necessary for TARPES measurements compared to static ARPES, since Ta_2NiSe_5 has a one-dimensional crystal structure, the large cleaved surface of the pristine Ta_2NiSe_5 enough for TARPES measurements was difficult to obtain. However, sufficiently large cleaved surfaces of 3% S-substituted Ta_2NiSe_5 and Ta_2NiS_5 could be obtained. This is why we used 3% S-substituted Ta_2NiSe_5 rather than the pristine Ta_2NiSe_5 for this study. The results of resistivity measurements by commercial physical property measurement system (PPMS, Quantum Design) for the sample characterization

is shown in Supplementary Fig. 1. The critical temperature of the structural transition of 3% S-substituted Ta_2NiSe_5 is determined to be ~ 321 K, whereas that of the pristine Ta_2NiSe_5 is ~ 325 K. Clean surfaces were obtained by cleaving *in situ*.

Photoemission measurements. In order to characterise the cleaved surfaces and compare with the previous results, temperature-dependent static ARPES measurements were performed with a He discharge lamp and a hemispherical electron analyser (Omicron-Scienta R4000) with the energy resolution of ~ 12.5 meV. The results were shown in Supplementary Fig. 2. We confirmed that the temperature dependence of the top of the flat band of the 3% S-substituted sample was almost the same as the previously reported one for the pristine samples, and thus that the electronic structure was almost not affected by the 3 % substitution. For the TARPES measurements, an extremely stable commercial Ti:Sapphire regenerative amplifier system (Coherent Astrella) with a centre wavelength of 800 nm ($h\nu = 1.55$ eV) and pulse duration of ~ 30 fs was used for the pump light. After generating a second harmonic (SH) via 0.2-mm-thick $\beta\text{-BaB}_2\text{O}_4$, the SH light was focused into a static gas cell filled with Ar and high harmonics were generated³⁰. We selected the ninth harmonic of the SH ($h\nu = 27.9$ eV) for the probe light by using a set of SiC/Mg multilayer mirrors³¹. The temporal resolution was evaluated to be ~ 80 fs from the TARPES intensity far above the Fermi level corresponding to the cross-correlation between pump and probe pulses. The energy resolution of the spectrometer was set to ~ 250 meV for the TARPES measurements.

Data availability. The data supporting the findings of this study are available from the corresponding author on request.

References

1. Mott, M. F., The transition to the metallic state, *Philos. Mag.* **6**, 287 (1961).
2. Cercellier, H. *et al.*, Evidence for an Excitonic Insulator Phase in 1T-TiSe₂, *Phys. Rev. Lett.* **99**, 146403 (2007).
3. Monney, C. *et al.*, Spontaneous exciton condensation in 1T-TiSe₂: BCS-like approach, *Phys. Rev. B* **79**, 045116 (2009).
4. Hellmann, S. *et al.*, Time-domain classification of charge-density-wave insulators, *Nat. Commun.* **3**, 1069 (2012).
5. Kogar, A. *et al.*, Signatures of exciton condensation in a transition metal dichalcogenide, *Science* **358**, 1314-1317 (2017)
6. Di Salvo, F. J. *et al.*, Physical and structural properties of the new layered compounds Ta₂NiS₅ and Ta₂NiSe₅, *J. Less-Common Metals* **116**, 51–61 (1986).
7. Sunshine, S. & Ibers, J., Structure and physical properties of the new layered ternary chalcogenides Ta₂NiS₅ and Ta₂NiSe₅, *Inorg. Chem.* **24**, 3611–3614 (1985).
8. Nakano, A. *et al.*, Pressure-induced coherent sliding-layer transition in the excitonic insulator Ta₂NiSe₅, *IUCrJ* **5** (2018).
9. Wakisaka, Y. *et al.*, H., Excitonic Insulator State in Ta₂NiSe₅ Probed by Photoemission Spectroscopy, *Phys. Rev. Lett.* **103**, 026402 (2009).
10. Kaneko, T., Toriyama, T., Konishi, T. & Ohta, Y., Orthorhombic-to-monoclinic phase transition of Ta₂NiSe₅ induced by the Bose-Einstein condensation of excitons, *Phys. Rev. B* **87**, 035121 (2013).
11. Seki, K. *et al.*, Excitonic Bose-Einstein condensation in Ta₂NiSe₅ above room temperature, *Phys. Rev. B* **90**, 155116 (2014).
12. Wakisaka, Y. *et al.*, Photoemission Spectroscopy of Ta₂NiSe₅, *J. Supercond. Nov. Magn.* **25**, 1231–1234 (2012).

13. Lu, Y. F. *et al.*, Zero-gap semiconductor to excitonic insulator transition in Ta₂NiSe₅, *Nat. Commun.* **8**, 14408 (2017).
14. Werdehausen, D. *et al.*, Coherent Order Parameter Oscillations in the Ground State of the Excitonic Insulator Ta₂NiSe₅, *Sci. Adv.* **4**, eaap8652.
15. Mor, S. *et al.*, Ultrafast Electronic Band Gap Control in an Excitonic Insulator, *Phys. Rev. Lett.* **119**, 086401 (2017).
16. Mor, S. *et al.*, Inhibition of the photoinduced structural phase transition in the excitonic insulator Ta₂NiSe₅, *Phys. Rev. B* **97**, 115154 (2018).
17. Werdehausen, D., Takayama, T., Albrecht, G., Lu, Y. F., Takagi, H., & Kaiser, S. Photo-excited dynamics in the excitonic insulator Ta₂NiSe₅, *J. Phys.: Condens. Matter* **30**, 305602 (2018).
18. Perfetti, L. *et al.*, Ultrafast Electron Relaxation in Superconducting Bi₂Sr₂CaCuO_{8+δ} by Time-Resolved Photoelectron Spectroscopy, *Phys. Rev. Lett.* **99**, 197001 (2007).
19. Mathias, S. *et al.*, Self-amplified photo-induced gap quenching in a correlated electron material, *Nat. Commun.* **7**, 12902 (2016).
20. Rohwer, T. *et al.*, Collapse of long-range charge order tracked by time-resolved photoemission at high momenta, *Nature* **471**, 490–493 (2011).
21. Larkin, T. I. *et al.*, Giant exciton Fano resonance in quasi-one-dimensional Ta₂NiSe₅, *Phys. Rev. B* **95**, 195144 (2017).
22. Imada, M., Fujimori, A., & Tokura, Y., Metal-insulator transitions, *Rev. Mod. Phys.* **70**, 1039-1263 (1998).
23. Miyasaka, S. *et al.*, Metal-Insulator Transition and Itinerant Antiferromagnetism in NiS_{2-x}Se_x Pyrite, *J. Phys. Soc. Jpn.* **69**, 3166-3169 (2000).
24. Mizokawa, T. *et al.*, Origin of the Band Gap in the Netative Charge-Transfer-Energy Compound NaCuO₂, *Phys. Rev. Lett.* **67**, 1638-1641 (1991).

25. Papalazarou, E. *et al.*, Coherent Phonon Coupling to Individual Bloch States in Photoexcited Bismuth, *Phys. Rev. Lett.* **108**, 256808 (2012).
26. Gerber, S. *et al.*, Direct characterization of photoinduced lattice dynamics in BaFe₂As₂, *Nat. Commun.* **6**, 7377 (2015).
27. Okazaki, K. *et al.*, Antiphase Fermi-surface modulations accompanying displacement excitation in a parent compound of iron-based superconductors, *Phys. Rev. B* **97**, 121107(R) (2018).
28. Zeiger, H. J., Vidal, J., Cheng, T. K., Ippen, E. P., Dresselhaus, G., & Dresselhaus, M. S., Theory for displacive excitation of coherent phonons, *Phys. Rev. B* **45**, 768-778 (1992).
29. Kim S. Y. *et al.*, Layer-confined excitonic insulating phase in ultrathin Ta₂NiSe₅ Crystals, *ACS Nano* **10**, 8888-8894 (2016).
30. Ishizaka, K. *et al.*, Femtosecond core-level photoemission spectroscopy on 1T-TaS₂ using a 60-eV laser source, *Phys. Rev. B* **83**, 081104 (2011).
31. Suzuki, H. *et al.*, Ultrafast melting of spin density wave order in BaFe₂As₂ observed by time- and angle-resolved photoemission spectroscopy with extreme-ultraviolet higher harmonic generation, *Phys. Rev. B* **95**, 165112 (2017).

Acknowledgements We would like to thank H. Fukuyama, and Y. Ohta for valuable discussions and comments. This work was supported by JSPS KAKENHI (Grant No. JP25220707 and JP26610095) and the Photon and Quantum Basic Research Coordinated Development Program from the Ministry of Education, Culture, Sports, Science and Technology, Japan. T. Someya acknowledges the JSPS Research Fellowship for Young Scientists.

Author Contributions K.O, Y.O., T. Suzuki, T.Y., M.O., T. Someya, S.M., and M.W. performed TARPES measurements. K.O. and Y.O. performed data analysis. M.F., T.K., N.I., and J.I. conducted

maintenance of HHG laser system and improvements of TARPES apparatus. Y.F.L., M.N., H.T., N.K., and H. S. grew high-quality single crystals and characterized them. K.O., Y.O, T. Suzuki, T.M., and S.S., wrote the manuscript. K.O., T.M., and S.S. designed the project. All authors discussed the results and contributed to the manuscript.

Additional Information

Supplementary Information accompanies this paper at <https://doi.org/xx.xxxx/xxx-xxx-xxxx-x>.

Competing Interests: The authors declare no competing interests.

Correspondence and requests for materials should be addressed to K.O. (okazaki@issp.u-tokyo.ac.jp) or S.S. (shin@issp.u-tokyo.ac.jp).

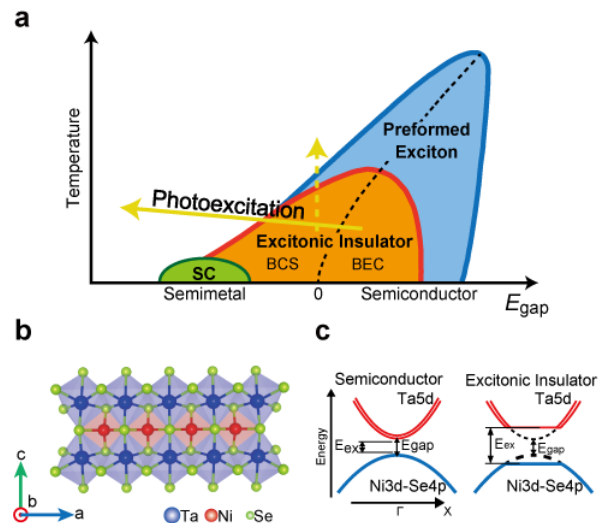


Figure 1 | Crystal and electronic structure of Ta_2NiSe_5 , and phase diagram of excitonic insulators. **a**, Phase diagram of Excitonic insulators. The solid arrow indicates the pathway for the photoinduced phase transition proposed in this study and the dashed arrow represents the effect of increasing the temperature. **b**, Crystal structure of Ta_2NiSe_5 . A quasi-one-dimensional structure is formed by a single Ni chain and two Ta chains along the a -axis. **c**, Schematic of the electronic structures of Ta_2NiSe_5 along the Γ -X direction in the semiconductor and excitonic insulator phases proposed by previous studies^{8–11}. When the exciton (which consists of an electron and a hole derived from doubly degenerate Ta 5d bands and the Ni 3d-Se 4p band) binding energy (E_{ex}) exceeds the band gap (E_{gap}), excitons are spontaneously formed and pure Bose-Einstein condensation of excitons arises with decreasing temperature.

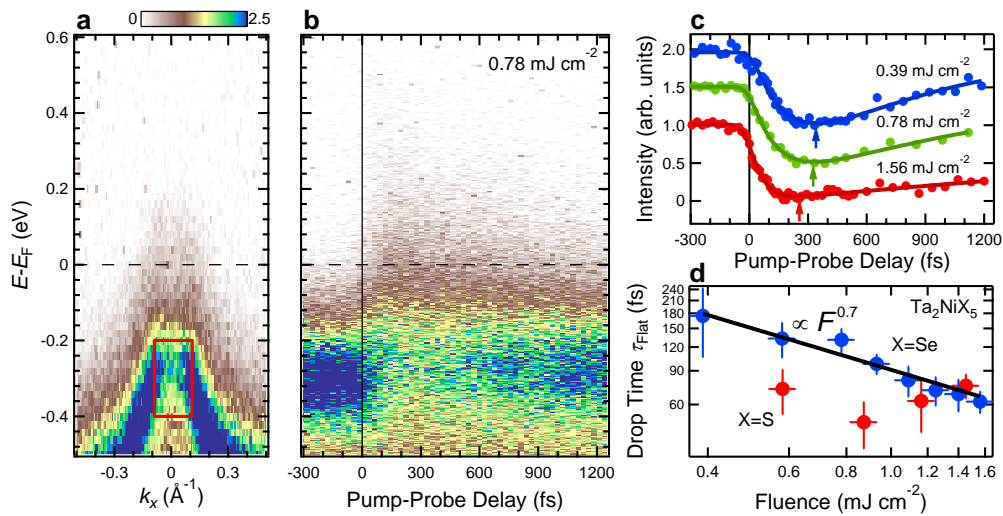


Figure 2 | Collapse of the flat band in Ta_2NiSe_5 . **a**, Energy-momentum map of $\text{Ta}_2\text{Ni}(\text{Se}_{0.97}\text{S}_{0.03})_5$ measured by using an XUV pulse (27.9 eV) before the arrival of the pump pulse (1.55 eV) at 100 K. **b**, TARPES spectrum at the Γ point, obtained with a pump fluence of 0.78 mJ cm^{-2} . **c**, Temporal evolution of the integrated TARPES intensity in the red square shown in **a** for different pump fluences. The arrows indicate the minimum values of the spectral weight. **d**, Extracted drop time of the flat band τ_{Flat} as a function of the pump fluence. Blue and red symbols corresponds to $\text{Ta}_2\text{Ni}(\text{Se}_{0.97}\text{S}_{0.03})_5$ and Ta_2NiS_5 , respectively. The error bars roughly correspond to the standard deviations.

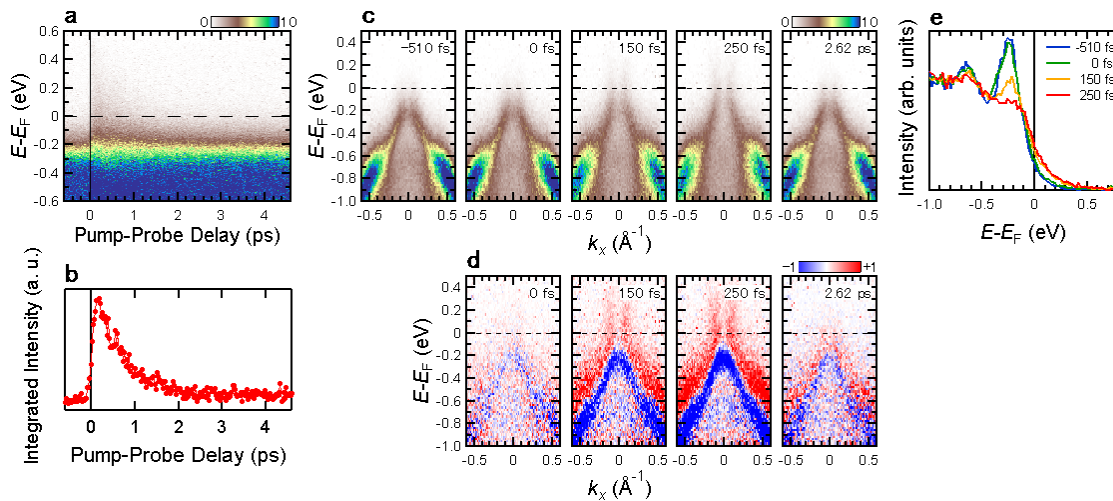


Figure 3 | Photoinduced transition from the insulator to the metallic phase observed with TARPES measurements. **a**, TARPES intensity map as a function of pump-probe delay and energy relative to E_F . This corresponds to the temporal evolution of the momentum-integrated EDC around the Γ point. **b**, Temporal evolution of the integrated intensity in the energy interval [0, 0.79] eV. **c**, TARPES snapshots acquired at increasing pump-probe delays (see also Supplementary Movie 1). **d**, Differential spectra of panel **c**, obtained by subtracting the spectrum averaged before t_0 . **e**, EDCs of the transient photoemission intensity integrated in the momentum range [-0.1, 0.1]. All time-resolved spectra were measured at 100 K with a pump fluence of 0.78 mJ cm^{-2} .

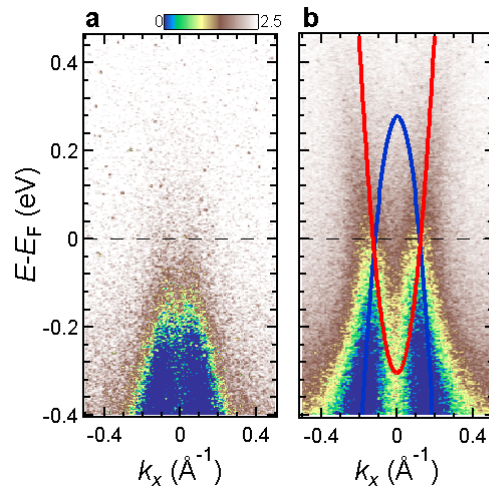
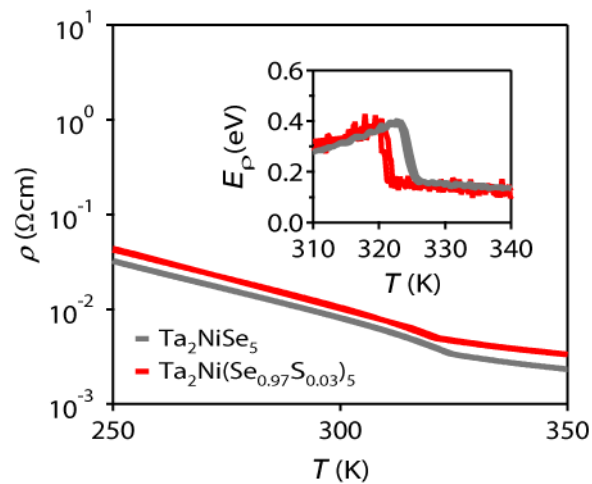
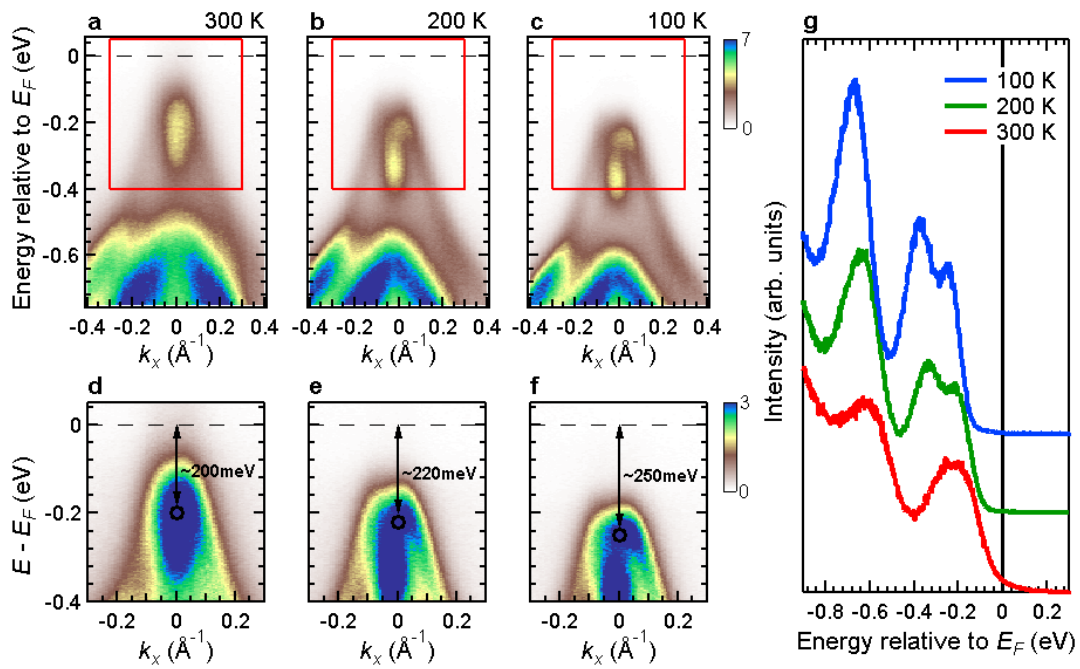


Figure 4 | TARPES spectra of Ta_2NiSe_5 before and after pumping. **a**, Energy-momentum ($E-k$) map before pumping, integrated in the time interval $[-0.29, 0]$ ps. **b**, Corresponding map of the transient states, integrated in $[0, 1.2]$ ps. Red and blue parabolas indicate the electron and hole bands crossing E_F in the non-equilibrium metallic state. These spectra were acquired with a pump fluence of 1.56 mJ cm^{-2} . Note that due to the worse energy resolution (~ 250 meV) compared to the static ARPES measurements shown in Extended Data Fig. 1, the $E-k$ map before pumping seems to have an intensity tail above E_F (see also Fig. 3e).

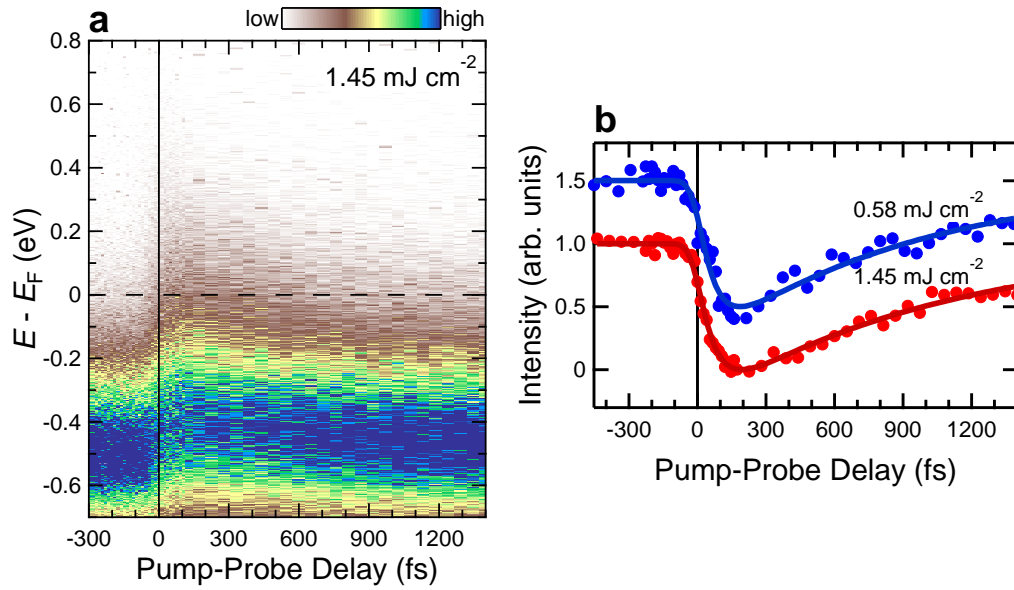
Supplementary Figures



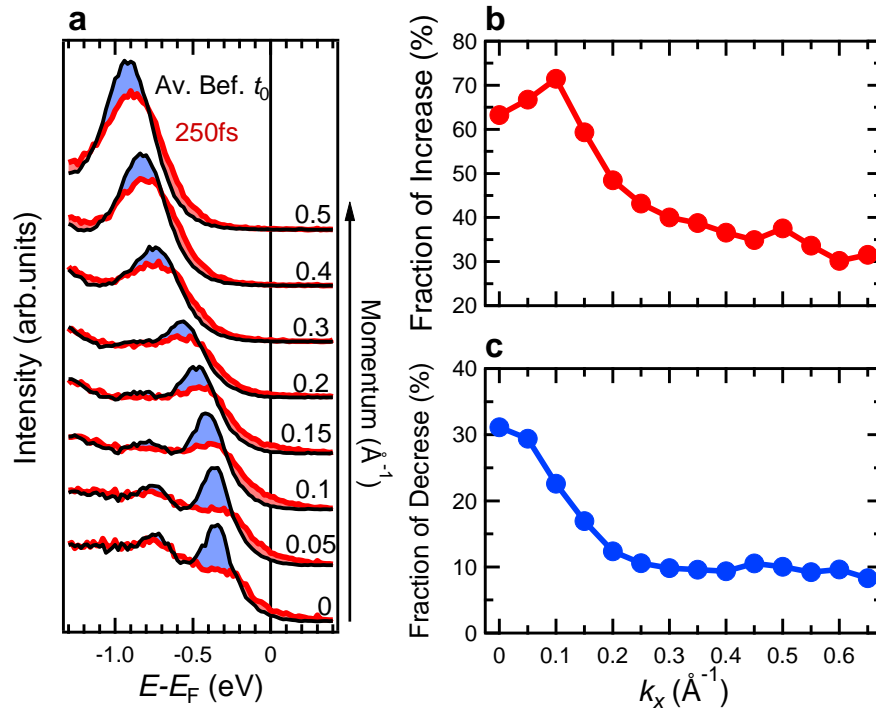
Supplementary Figure 1 | Resistivity data of Ta_2NiSe_5 and $\text{Ta}_2\text{Ni}(\text{Se}_{0.97}\text{S}_{0.03})_5$. The results for the pristine and substituted samples are plotted by grey and red lines, respectively. The inset shows the activation energy ($E_p = -k_B T^2 (\partial \ln \rho / \partial T)$) deduced from the resistivity data. Compared to the pristine sample, the critical temperature of the substituted sample is lower by ~ 4 K, but the activation energy is almost the same between these two compositions.



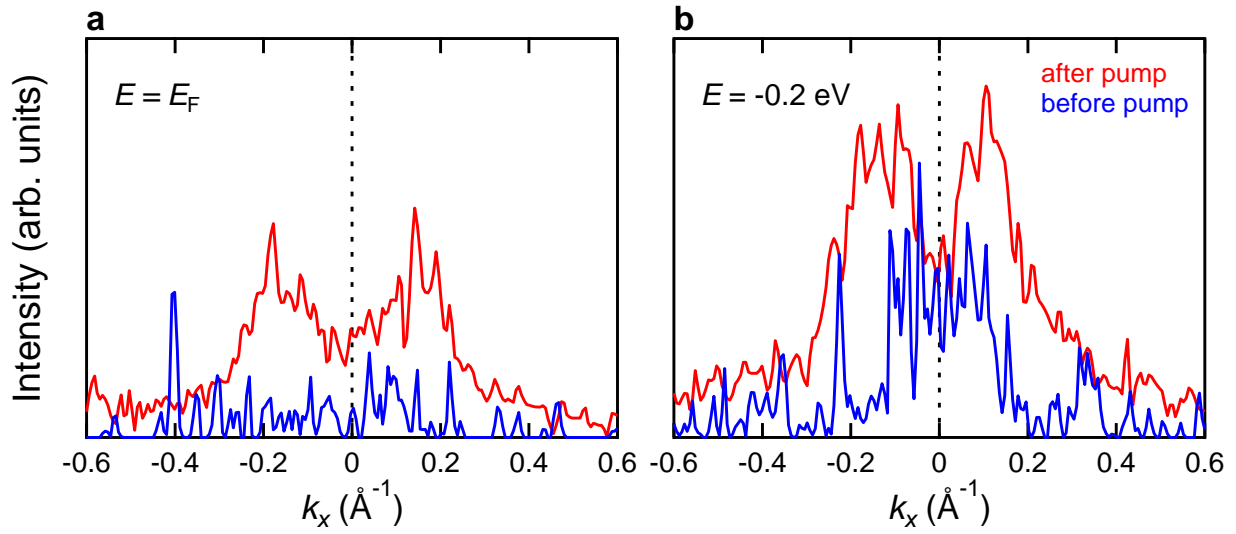
Supplementary Figure 2 | Temperature-dependent ARPES spectra of $\text{Ta}_2\text{Ni}(\text{Se}_{0.97}\text{S}_{0.03})_5$. **a–c**, Energy vs. momentum ($E-k$) images around the Γ point taken with He $I\alpha$ resonance line (21.2 eV) at 300, 200, and 100 K, respectively. **d–f**, Magnifications of **a–c** around E_F . **g**, Temperature-dependent EDCs around the Γ point.



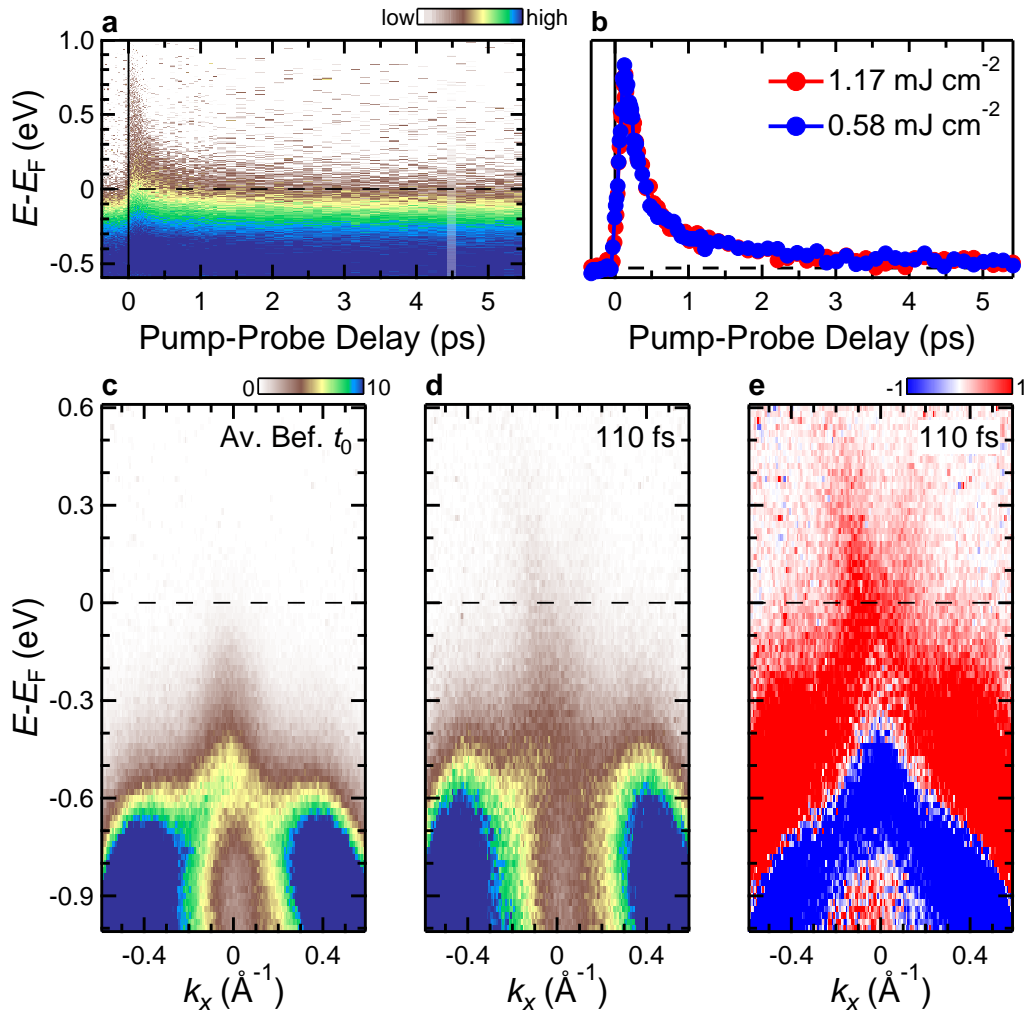
Supplementary Figure 3 | Pump fluence dependence of Ta₂NiS₅. **a**, TARPES intensity map of Ta₂NiS₅ as a function of pump-probe delay and energy relative to E_F taken with a pump fluence of 1.45 mJ cm⁻². **b**, Temporal evolution of the TARPES intensity integrated in [-0.7, -0.5] eV for different pump fluences.



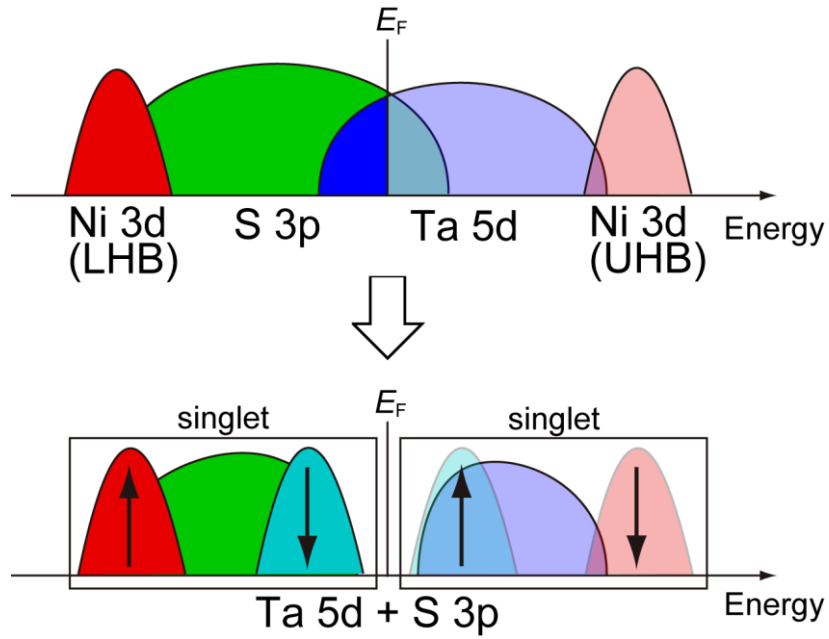
Supplementary Figure 4 | Comparison of EDCs before and after pumping at various momenta. **a**, EDCs before and after pumping at various momenta. The EDCs before pumping were averaged for several EDCs and the EDCs after pumping were measured 250 fs after pumping. **b**, **c**, Momentum dependence of the fractions of increase and decrease defined by Supplementary Eqs. 1 and 2, respectively. These plots roughly correspond to the MDC at E_F after pumping and the MDC at the top of the flat band before pumping, respectively.



Supplementary Figure 5 | Comparison of MDCs before and after pumping. a, b, MDCs before and after pumping at E_F and $E = -0.2$ eV (top of the flat band before pumping), respectively, from the TARPES spectra shown in Fig. 4. The energy integration window is ± 0.1 eV.



Supplementary Figure 6 | TARPES spectra of Ta₂NiS₅. **a**, Photoemission intensity map of Ta₂NiS₅ as a function of energy and pump-probe delay. **b**, Temporal evolution of the integrated intensity in the energy interval [0, 1] eV, measured with pump fluences of 1.17 and 0.58 mJ cm⁻². **c**, **d**, TARPES intensity maps as a function of energy and momentum before pumping and at 110 fs after pumping, respectively (see also Supplementary Movie 2). **e**, Difference between the TARPES spectra shown in **c** and **d**. The red and blue regions correspond to the spectra appearing and disappearing after pumping, respectively.



Supplementary Figure 7 | Schematic energy diagram for the possible ground-state electronic configurations of Ta_2NiS_5 . Ta 5d electrons in the double chains form singlet states with the localized $d^0 \underline{L}$ state via hybridization with the S 3p orbitals, and the ground state of Ta_2NiS_5 can be viewed as a valence-bond insulator. LHB and UHB denote “lower Hubbard band” and “upper Hubbard band”, respectively.

Supplementary Notes

Definition of fractions of increase and decrease

Supplementary Figure 4 shows the EDCs of $\text{Ta}_2\text{Ni}(\text{Se}_{0.97}\text{S}_{0.03})_5$ before and after pumping at various momenta. It is obvious that the spectral weight of the EDC peak corresponding to the flat band before pumping is shifted to the higher energies with increasing momentum. These two EDCs intersect at the lower- and higher-energy sides of the flat-band peak at the points of ω_1 and ω_2 , respectively. Using ω_1 and ω_2 , the fractions of increase and decrease plotted in Supplementary Fig. 4b and 4c are defined as follows:

$$\text{fraction of increase} = \int_{\omega_2}^{\infty} I(\omega, t = 250 \text{ fs}) d\omega / \int_{\omega_2}^{\infty} I(\omega, t < 0) d\omega - 1, \quad (1)$$

$$\text{fraction of decrease} = 1 - \int_{\omega_1}^{\omega_2} I(\omega, t = 250 \text{ fs}) d\omega / \int_{\omega_1}^{\omega_2} I(\omega, t < 0) d\omega. \quad (2)$$

The fraction of increase has its maximum at 0.1 \AA^{-1} , which roughly coincides with the location of the Fermi momentum in the photoinduced metallic state. On the other hand, the fraction of decrease has its maximum at the BZ centre, which corresponds to the location of the flat band peak. Therefore, these plots roughly correspond to the MDCs after and before pumping.

Quantitative evaluation of gap quenching time

We used a method similar to that described in Ref. 1 to quantitatively evaluate the number of absorbed photons per Ni atom and the plasma response time after photoexcitation by an 800 nm (1.55 eV) pump pulse.

First, we consider an incident pump fluence of $1 \text{ mJcm}^{-2} = 4 \times 10^{15}$ photons per cm^2 . It has been reported² that the optical conductivity σ and dielectric constant ϵ_r of Ta_2NiSe_5 at 1.55 eV are $\sim 3000 \text{ \Omega}^{-1}\text{cm}^{-1}$ and 10, respectively, from which an optical reflectance of 42.8% and an absorption coefficient of $3 \times 10^5 \text{ cm}^{-1}$ were obtained. From these values, the absorbed photon density was evaluated to be 7×10^{20} photons cm^{-3} . Considering that Ta_2NiSe_5 has a unit cell volume of 701 \AA^3 and a density of 4 Ni atoms per unit cell, this is equivalent to 0.12 photons per Ni atom.

In the presence of photoexcited electrons and holes, the plasma frequency ω_p is given by

$$\omega_p = \sqrt{\frac{e^2}{\epsilon_0 \epsilon_r} \times \left(\frac{n_h}{m_h^*} + \frac{n_e}{m_e^*} \right)} \quad (3)$$

where n_h and n_e are the carrier numbers, m_h^* and m_e^* are the effective masses of the excited holes and electrons, respectively, e is the elemental charge, and ϵ_0 is the electric constant. The TARPES image of Ta_2NiSe_5 in the photoinduced metallic phase shows that the holes and electrons are fully compensated ($n_h = n_e$) and the effective

mass of the hole and electron bands is almost equal ($m_{\text{h}}^* = m_{\text{e}}^* = 0.37m_0$, where m_0 is the bare electron mass). Based on these results, the observed quenching time of the flat band $\tau_{\text{Flat}} \approx 90$ fs (corresponding to $\omega_{\text{p}} \approx 45$ meV) at a pump fluence of 1 mJ cm^{-2} corresponds to a quantum efficiency (fraction of the number of electron-hole pairs per absorbed photon) of $\sim 1.6\%$. However, the effective mass of the bands emerging in the photoinduced metallic state might be inappropriate for the evaluation of the number of photoexcited electron-hole pairs. If we use the effective mass of the flat band before photoexcitation ($\sim 5 m_0$) and assume a quantum efficiency of 21.5% , the observed quenching time of the flat band $\tau_{\text{Flat}} \approx 90$ fs at 1 mJ cm^{-2} can be deduced, which is more reasonable.

Supplementary References

1. Hellmann, S. *et al.*, Time-domain classification of charge-density-wave insulators, *Nat. Commun.* **3**, 1069 (2012).
2. Larkin, T. I. *et al.*, Giant exciton Fano resonance in quasi-one-dimensional Ta_2NiSe_5 , *Phys. Rev. B* **95**, 195144 (2017).